Nano Materials Science 3 (2021) 412–419

Contents lists available at ScienceDirect

Nano Materials Science

journal homepage: www.keaipublishing.com/cn/journals/nano-materials-science/

Selected gas response measurements using reduced graphene oxide decorated with nickel nanoparticles

Ilka Simon [a], Yulyan Haiduk [b], Rolf Mülhaupt [c], Vladimir Pankov [b,*], Christoph Janiak [a,**]

[a] Institut für Anorganische Chemie und Strukturchemie, Heinrich-Heine-Universität Düsseldorf, 40204, Düsseldorf, Germany
[b] Chemical Faculty, Belarusian State University, Lenningradskaya Str. 14, 220050, Minsk, Belarus
[c] Freiburg Materials Research Center and Institute for Macromolecular Chemistry, Albert-Ludwigs-University, Freiburg, 79104, Freiburg, Germany

ARTICLE INFO

Keywords:
Nickel nanoparticles
Reduced graphene oxide
Gas sensing
Nanocomposite

ABSTRACT

The work reports the synthesis of nickel nanoparticles supported on thermally reduced graphene oxides (rGO) in the ionic liquid [BMIm][NTf_2] through microwave decomposition reaction. Ni@rGO with the polymer poly(3,4-ethylenedioxythiophene):poly(styrene sulfonate) (PEDOT:PSS) as binder was positively tested for its response towards the oxidizing gas nitrogen dioxide (10 ppm in air), the reducing gas carbon monoxide (3000 ppm in N_2) and the volatile organic compound (VOC) acetone (35,000 ppm in air). The results from different gases were compared at different temperatures with the best results for NO_2 at 200 °C. Additionally, it is shown for NO_2 gas that the Ni@rGO-PEDOT:PSS polymer composite gives better results than the rGO-PEDOT:PSS polymer composite. After the heat treatment the oxidation state of pure nickel nanoparticles were confirmed by powder diffraction.

1. Introduction

Air pollution is a highly discussed topic for being one of the biggest risks for human health and the environment in recent years [1]. Gaseous pollutants that are in the focus include oxidizing gases like nitrogen oxide (NO_2, NO, N_2O), reducing gases like carbon monoxide (CO) and volatile organic compounds like acetone [2]. These gases are either industrial origins or produced by burning fossil fuel and biomass [3,4]. To detect even small quantities of these harmful gases, highly sensitive and selective gas sensors are needed [5].

Carbon based sensor materials show promising results for all kinds of gases [6]. The advantages of graphene based materials like graphene (G) and graphene oxide (graphite oxide, GO) are the high surface area, high chemical and thermal stability [7]. For gas sensing the right amount of oxygen functionalities on the graphene surface is necessary. With graphene having only a few functional groups on its surface [8] and GO having numerous functional groups [9], the best graphene based sensors are using reduced graphene oxide (rGO) [10]. rGO can either be chemically or thermally reduced from graphene oxide [11]. This results in a partial removal of oxygen groups from the surface, creation of defects and vacancies, restoring the good conductivity close to pristine graphene [10]. To gain a high surface area the graphene sheets need to be exfoliated. This can be achieved by mechanical exfoliation or sonification in water [12]. Additionally stabilizers and surfactants are used to prevent backward aggregation of the exfoliated sheets [13]. Exfoliation and stabilization of the graphene sheets can also be achieved in a one-step solution using ionic liquids (ILs) [14]. The close surface tension of ionic liquids to the surface energy of graphite leads to the exfoliation. The ionic nature of the ionic liquids helps with the stabilization of the exfoliated sheets. The ionic liquid [BMIm][NTf_2] is utilized for the exfoliation of graphite [15]. Whereas [BMIm][BF_4] was tested in the stabilization of rGO [13]. [BMIm][PF_6] [12] and [HMIm][PF_6] [16] are used for the stabilization of graphene. A high surface area per atom results in a high electron transport along the sheets, which leads to rapid and high response to gas molecules even at room temperature [17]. rGO is a *p*-type semiconductor [18]. Measurement in the resistance mode shows for the interaction of a *p*-type semiconductor with a reducing gas an increase in resistance because the negative charge reduces the positive charge carrier (hole) concentration. The interaction with an oxidizing gas leads to an increase of positive holes which is shown in a decrease in the measured resistance [17].

The combination of nanoparticles with graphene materials enhance the sensitivity and selectivity towards target gases. These graphene-nanoparticle hybrid materials can either be graphene-nanoparticles

* Corresponding author.
** Corresponding author.
E-mail addresses: pankov@bsu.by (V. Pankov), janiak@uni-duesseldorf.de (C. Janiak).

https://doi.org/10.1016/j.nanoms.2021.03.004
Received 17 December 2020; Accepted 9 March 2021
Available online 18 May 2021

composites where nanoparticles are decorated on top of the graphene sheets or graphene-encapsulated nanoparticles, where nanoparticles are wrapped or coated with graphene. Graphene nanoparticle composites can be synthesized in situ by growing nanoparticles on the graphene surface or ex situ by attaching pre-synthesized nanoparticles to the graphene surface [19]. Functional groups on the surface of the graphene material have excellent anchoring abilities for the nanomaterials like metallic nanoparticles [20]. Synthesis via in situ reduction can be executed by a one-step method where metal precursors and GO sheets are mixed and simultaneously reduced. Nickel nanoparticles decorated graphene can be synthesized simultaneously from GO and nickel (II)-precursor material using a reducing agent [21].

With the use of microwave irradiation, reducing agents and stabilizing molecules small nanoparticles with a narrow size distribution can be obtained. The use of ionic liquids as solvents has additional advantages because they are highly microwave active, can stabilize nanoparticles and can further exfoliate the graphene sheets without the use of additional stabilizing and reducing agents [22,23]. The synthesis of nickel nanoparticles can be achieved through thermal decomposition [24] or reductive hydrogenation [25]. With the precursor $Ni(COD)_2$ nickel nanoparticles of 10 nm and bellow can be synthesized in different ionic liquids without the addition of stabilizing or reducing agents using microwave irradiation [26]. In previous works we and others had successfully deposited ruthenium- [27–29], rhodium- [27], iridium- [30], palladium- [27], platinum- [31], and various metal fluoride nanoparticles [32] on thermally reduced graphene/graphite oxide. The Ru-, Rh- and Ir-nanoparticle@rGO composites were reusable and highly active hydrogenation catalysts towards cyclohexene and benzene [27,29,30].

Gas sensing with metal nanoparticles decorated on top of graphene materials are known for noble metals like palladium and platinum. Pt-nanoparticles [33] and Pd-nanoparticles [34] decorated on pristine graphene improves the sensitivity towards the hydrogen gas. For NO gas sensing Pd-nanoparticles decorated on rGO is the better gas sensor for small concentrations of NO gas at room temperature. For higher concentrations of NO gas a graphene-Pd-rGO sensor is superior [35]. Ni-nanoparticles individually decorated on the surface of graphene nanosheets improve the electrochemical sensing of carbohydrates in comparison to graphene or nickel nanoparticles alone [36]. In the sensing of 10 ppm NH_3 gas the response time of Ni@graphene is one third of that of pure graphene [37]. A nickel-graphene gas sensor was used to test the influence of thermal annealing in the sensing of NH_3 gas. With increased temperatures from 300 °C to 600 °C the response of the contact resistance increases from 23% to 56%, the channel resistance dropped from 23% to 6%. The response and recovery times were decreased significantly after annealing at 600 °C [38].

In this work a composition material of nickel nanoparticles decorated on rGO was coated on a ceramic substrate (Al_2O_3) with the polymer poly(3,4-ethylenedioxythiophene):poly(styrene sulfonate) (PEDOT:PSS) as binder and the response towards different gases at different temperatures were evaluated. The selected gases are oxidizing gas NO_2 (10 ppm in air), the reducing gas CO (3000 ppm in N_2) and the volatile organic compound (VOC) acetone (35,000 ppm in air). A comparison of rGO-PEDOT:PSS polymer composite vs. Ni@rGO-PEDOT:PSS polymer composite was made for NO_2.

2. Materials and methods

2.1. Synthesis

All synthesis experiments were performed under nitrogen (grade 99.998 vol.-%) or argon (99.998 vol.-%) with the use of Schlenk ware or an MBraun Glovebox. The precursor compounds and the nickel nanoparticles are air and moisture sensitive. The solvents acetonitrile, *n*-hexane and methylene chloride were dried with over activated aluminum oxide in an MBraun solvent purification device. The solvents 1-methylimidazole, 1-chlorobutane were dried and distilled under nitrogen from 4 Å molecular sieve and stored over fresh 4 Å molecular sieves under N_2. The water content of the dried solvents was verified to be below 10 ppm through a coulometric Karl Fischer titration with an ANALYTIK JENA AQUA 40.00 titrator. $Ni(COD)_2$ was obtained from ABCR, stored at −4 °C and used as such.

2.1.1. Preparation of the ionic liquid [BMIm][NTf$_2$]

Following established literature syntheses, the reaction of 1-methylimidazole with 1-chlorobutane gave [BMIm][Cl] which upon anion exchange with $LiNTf_2$ yielded the ionic liquid [BMIm][NTf_2] [39,40]. Water was removed from [BMIm][NTf_2] in a turbo molecular pump vacuum (10^{-7} mbar) at 80 °C for three days. Coulometric Karl Fischer titration (ANALYTIK JENA AQUA 40.00) gave a residual water content below 10 ppm. The purity of the product was verified by ^1H and ^{13}C NMR. The anion and overall IL purity was determined to 99.9% by ion chromatography with a Dionex ICS-1100 (column IonPac® AS22, 4 × 250 mm).

2.1.2. Preparation of rGO

Thermally reduced graphene oxide (rGO) was prepared in a two-step oxidation/thermal reduction process from natural graphite (type KFL 99.5 from AMG Mining AG, formerly Kropfmühl AG, Passau, Germany) as raw material. The graphite oxidation process of Hummers and Offeman was employed [41]. The rGOs was provided by the group of Prof. Rolf Mülhaupt, University of Freiburg. Details for the synthesis and characterization of rGO were reported before [32]. The intermediate graphite oxide, GO was reduced at 400 °C and had an elemental analysis of ~80% C and ~0.8% H. The oxygen content (~19%) was taken as the difference to 100%. rGO was dried in a turbo-molecular pump vacuum at $5{\cdot}10^{-7}$ mbar at 100 °C for several days.

2.1.3. Preparation of Ni@rGO

$Ni(COD)_2$ (49.2 mg, 0.178 mmol) and rGO (10 mg) were stirred in the IL [BMIm][NTf_2] (2.0 g) for 2 h in septum-sealed 10 mL CEM microwave-vessels under argon atmosphere. Microwave irradiation (CEM Discover microwave) for 10 min at the power of 50 W at an upper limit temperature of 230 °C then yielded a black dispersion of Ni-nanoparticles on rGO, dispersed in the ionic liquid.

2.2. Characterization

Powder X-ray diffraction, PXRD data were measured on a Bruker D2 Phaser using a flat, low-background Si sample holder and Cu–Kα radiation ($\lambda = 1.54182$ Å, 35 kV). The scan time from 5 to 100° 2-theta was 1 h. Nanoparticle samples had been precipitated from the Ni@rGO/ionic liquid dispersion with acetonitrile and the ionic liquid was removed by washing several times with acetonitrile.

Flame atomic absorption spectroscopy, F-AAS for nickel quantification was carried out on a PerkinElmer PinAAcle 900T with an air-acetylene flame. Samples were dissolved by refluxing twice in hot aqua regia (30 mL) and evaporation to dryness. The residues were re-dissolved in aqua regia, filtered and diluted with water to a total volume of 1000 mL to reach a nickel concentration in the optimal concentration range.

Transmission electron microscopy, TEM was performed with a FEI Tecnai G2 F20 electron microscope [42] operated at 200 kV accelerating voltage or a FEI Titan 80-300 TEM operated at 300 kV accelerating voltage [43]. TEM images were recorded with a Gatan UltraScan 1000P detector. *Energy-dispersive X-ray spectroscopy, EDX* mapping for spatially resolved elemental analysis was done with an exposure time of 3 min. The estimated standard deviation for the element contributions in a high-resolution EDX scan was 10–15%. TEM samples were prepared on 200 μm carbon-coated copper grids by drop-casting an acetonitrile diluted Ni@rGO/ionic liquid dispersion. Afterwards the ionic liquid was removed by washing with acetonitrile. The size distribution histogram was derived from at least 50 individual particles whose size was

measured manually or with the aid of the Gatan Digital Micrograph software.

2.3. Gas sensing tests

Gas sensing properties of Ni@rGO on a ceramic substrate (Al_2O_3, area 3 × 4 mm) were determined in a home-designed flow type sensing measurement system inside an aluminum chamber with precisely controlled temperature and atmosphere. Pt electrodes were attached to the substrates. The area of the working zone was 2 × 2 mm, the distance between the electrodes was 0.1 mm. The Pt electrodes were prepared from a sputtered Pt film, using photolithography and lift off processes. A paste based on Ni@rGO powder with the addition of a 2 wt.-% aqueous solution of the conductive polymer poly(3,4-ethylenedioxythiophene):poly(styrene sulfonate) (PEDOT:PSS) was applied to the working area of the substrates by screen-printing method. Screen-printing involves pushing an ink through a porous layer or mesh, which is suitably masked to produce the required layout on the substrate. Samples were dried at 25 °C. To investigate the sensing properties the sensors were introduced in a test chamber with a volume of 120 cm^3 with control of the sensor temperature under variable gas concentration (see Supp. Info. for further details). Dry air was used as a reference gas.

3. Results and discussion

3.1. Ni@rGO synthesis and characterization

The precursor bis(cyclooctadiene)nickel(0) [$Ni(COD)_2$] is well-suited and has been described before for the soft wet-chemical synthesis of nickel nanoparticles in ionic liquids (IL) [26]. Microwave irradiation is the heating method of choice for ionic liquids to induce the thermal decomposition of various organometallic complexes. The ionic charge, polarity and dielectric constant of ionic liquids lead to very high microwave absorption efficiencies which result in rapid and effective heating by microwave irradiation [44,45,46]. During formation of the nanoparticles the ionic liquid stabilizes them and can also assist in the further exfoliation of the rGO sheets [47].

The hydrophobic ionic liquid 1-butyl-3-methylimidazolium bis(trifluoromethylsulfonyl)imide [BMIm][NTf_2] was chosen as reaction medium as it can be readily prepared with a low water content, unlike [BF_4]-containing ionic liquids. Moreover, the [NTf_2]$^-$ anion is thermally and hydrolytically very stable without the danger of forming NiF_2, as this may occur in fluorous ionic liquids with [BF_4], [PF_6] or [CF_3SO_3] anions [32,48,49].

The oxidation of graphite with $NaNO_3$ and $KMnO_4$ in conc. H_2SO_4 by the Hummers and Offeman process [41] yields graphite oxide, GO. When this GO is rapidly heated to several hundred degree centigrade under a nitrogen atmosphere, the introduced oxygen (epoxy, alcohol, aldehyde) groups are partially removed again with concomitant formation of CO and CO_2 gas. This thermal reduction process also exfoliates the now defective graphite/graphene sheets [50] and gives (thermally) reduced graphite/graphene oxide (rGO). The amount of remaining oxygen functionalities can be adjusted by the reduction temperature. The lower the temperature, the more oxygen is retained in the rGO. The more oxygen functionalities the better is the dispersibility of rGO in polar solvents, *e.g.*, in water or acetone [51] and the better the anchoring and interaction with metal nanoparticles on the rGO surface. Totally reduced graphene surfaces do not provide functional sites for the nucleation and growth of metal nanoparticles [31,52]. It is its surface functionalization which renders rGO as a good support material for metal nanoparticle-graphene composites with high metal content [53].

Neat nickel nanoparticles were prepared before in [BMIm][NTf_2] (from $Ni(COD)_2$) and had an average diameter of 11 ± 2 nm [26]. Nickel nanoparticles from nickel (II)sulfate deposited on pristine graphene sheets could be obtained with a size and dispersion of 35 ± 5 nms [21].

Because of the oxyphilic nature of nickel metal nanoparticles it is important to work under water-free conditions. Therefore, all reactants (rGO, IL) were carefully dried at elevated temperature under ultra-high turbo-molecular pump vacuum ($5{\cdot}10^{-7}$ mbar) for several days and solvents were dried over activated aluminum oxide. Wherever possible the residual water content was controlled by Karl-Fischer titration. When for example the rGO was dried under normal oil-pump vacuum (10^{-3} mbar) only, nickel oxide, NiO was formed upon decomposition of $Ni(COD)_2$ in the presence of this obviously still not sufficiently dried rGO (see Supp. Info.)

The Ni@rGO composite was prepared by microwave induced heating from the decomposition of $Ni(COD)_2$ in the presence of rGO in [BMIm][NTf_2] from which a dispersion of 0.5 wt.-% nickel nanoparticles and 0.5 wt.-% rGO in the ionic liquid was then obtained. The amount of 0.5 wt.-% rGO could not be exceeded as otherwise the ionic liquid dispersion would become too highly viscous.

The powder X-ray diffraction (PXRD) pattern shows the reflexes for hexagonal nickel (Fig. 1a). Transmission electron microscopy (TEM) images exhibit spherical and partly facetted nickel nanoparticles (Fig. 1b). The particles have a size of 25 ± 5 nm (Fig. 1c). The particle size of Ni@rGO had increased in comparison to neat nickel nanoparticles from [BMIm][NTf_2] (11 ± 2 nm) [26].

The TEM-images reveal the well-known wrinkled structure of rGO (Fig. 2a). The nickel nanoparticles were deposited on top and in between the rGO sheets (Fig. 2b). There was no indication of non-supported particles elsewhere on the grid. rGO sheets were already used successfully as supporting material for various metal [29–31] and metal fluoride [32] nanoparticles. As an alternative to rGO sheets supporting nanoparticles, the rGO could also form a cladding structure surrounding the nanoparticles [54]. The close-up TEM-image show, however, that there is no indication of a cladding structure of rGO around the nickel nanoparticles (Fig. 2c).

From atomic absorption spectroscopy (AAS) the nickel content for Ni@rGO was determined to 8 wt.-%. A metal loading on reduced graphene oxides between 5 and 20% has been reported [32].

In order to investigate phase changes occurring with the nickel particles in the Ni@rGO composite after its heat treatment in the study of sensor properties (250 °C), the following model experiment was performed. The original Ni@rGO composite was annealed at a temperature of 250 °C for 2 h. The determined powder pattern shows reflexes for hexagonal nickel (Fig. 3).

3.2. Gas sensing tests with Ni@rGO on Al_2O_3 substrates

To evaluate the gas response of Ni@rGO, ceramic substrates (Al_2O_3) were used. Alumina substrates are most commonly used for sensors, because the sensor substrate must have a high resistance, high thermal conductivity and chemical inertness [55–57]. The tested gases were the oxidizing gas NO_2 (10 ppm in air), the reducing gas CO (3000 ppm in N_2) and the VOC acetone (35,000 ppm in air). It is known that semiconductor sensors are generally characterized by a higher sensitivity to oxidizing gases than to reducing gases [58]. Therefore, higher concentrations of CO and acetone were applied. Dry air was used as a reference gas. The electrical resistance was measured for the testing gas mixture and air. *Sensor response (S)* was calculated according to equations with R_{air} as resistance of the sensor element in the air and R_{gas} as resistance in the test gas mixture [3].

$S = (R_{air} / R_{gas}) * 100\%$, for reducing gas mixtures.

$S = (R_{gas} / R_{air}) * 100\%$, for NO_2 / air mixture.

The CO/air mixture was measured in flow mode. In the case of NO_2 and acetone, a static mode was used, in which a given amount of gas was introduced into a sealed chamber. The chamber volume was 120 cm^3. The response time can be seen in the presented figures.

For the manufacture of efficient modern gas sensors, it is customary to use rGO either as part of compositions with conducting polymers to

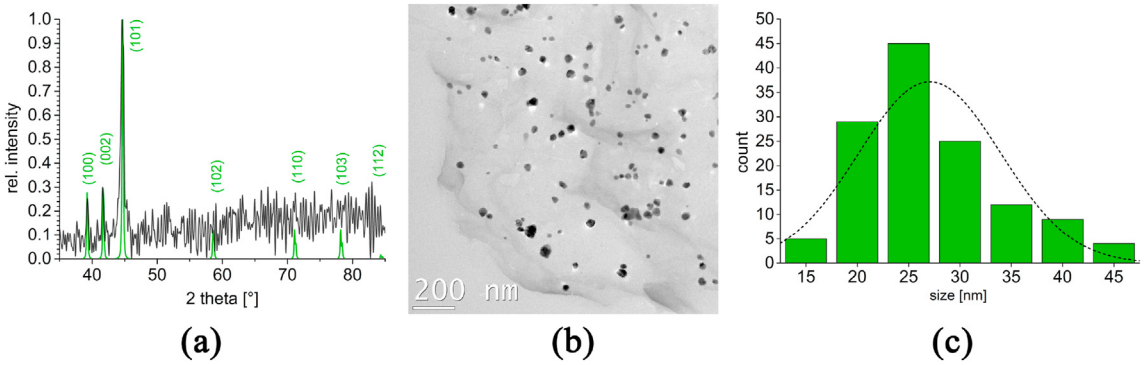

Fig. 1. (a) Powder X-ray diffraction pattern, (b) TEM-image and (c) particle size distribution of Ni@rGO from the decomposition of $Ni(COD)_2$ in the presence of carefully dried rGO in [BMIm][NTf_2] (green reflexes in the PXRD pattern in (a) indicate Ni metal from COD 9008509, Ni space group: *P* $6_3/mmc$). Particle size distribution in (c) is 25 ± 5 nm.

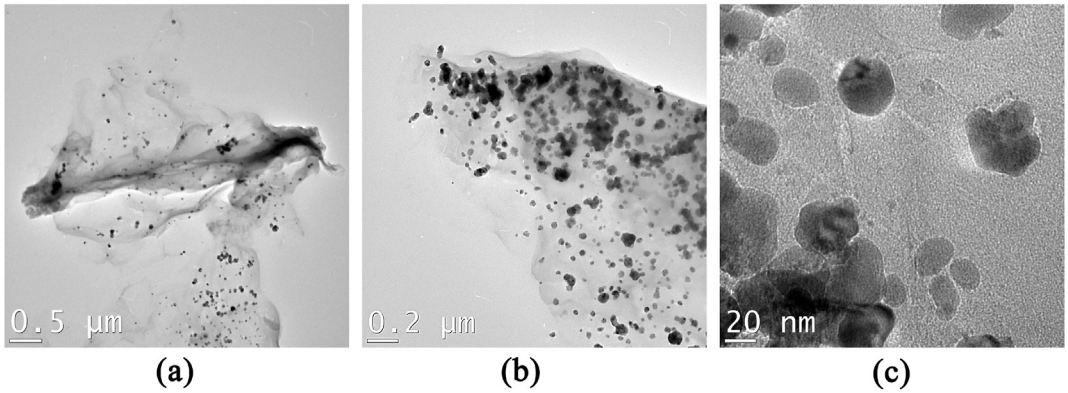

Fig. 2. TEM-images of Ni@rGO from the decomposition of $Ni(COD)_2$ in the presence of carefully dried rGO in the IL [BMIm][NTf_2]. (a) Wrinkled structure of rGO with nickel nanoparticles. (b) Nickel nanoparticles supported on top and in between the rGO sheets. (c) Close-up of nickel nanoparticles.

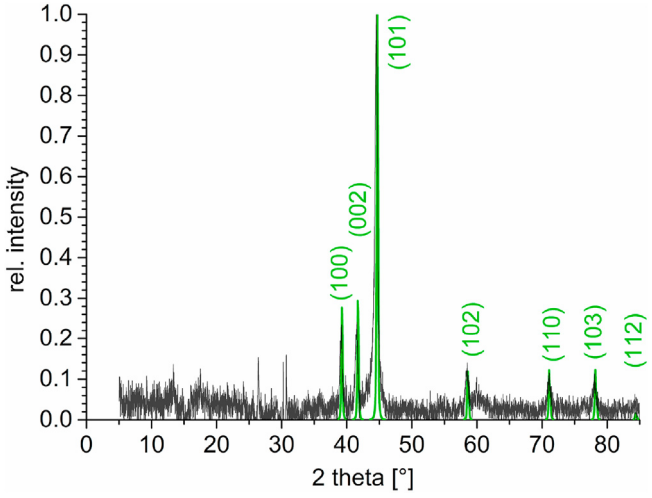

Fig. 3. Powder X-ray diffraction pattern of nickel Ni@rGO from 0.5 wt.-% dispersion of from $Ni(COD)_2$ in [BMIm][NTf_2] after annealing at 250 °C for 2 h (green reflexes in the PXRD pattern indicate Ni metal from COD 9008509, Ni space group: *P* $6_3/mmc$).

ensure the formation of a conductive film coating at low temperatures (up to 200 °C), or as part of a composition of rGO with oxides [59]. The composition of rGO with oxides are applied as a layer onto an inorganic substrate. Sensors based on electrically conductive polymers have a significantly lower operating temperature of 20–80°C versus 130–350 °C for composition of rGO with oxides [59]. PEDOT:PSS was used as a binder that ensures the adhesion of rGO powder to the substrate, and also provides electrical conductivity between rGO sheets in the layer. During the measurements, the samples were thermostated in the temperature range of 20–220 °C. The temperature dependence of the electrical resistance of the rGO-polymer composite is shown in Fig. 4.

It turned out that the electrical resistance of the compositions is sensitive to low concentrations of NO_2 at temperatures of less than 100°C (Fig. 5a). Within 3 min of exposure to a mixture of 10 ppm NO_2 in air at

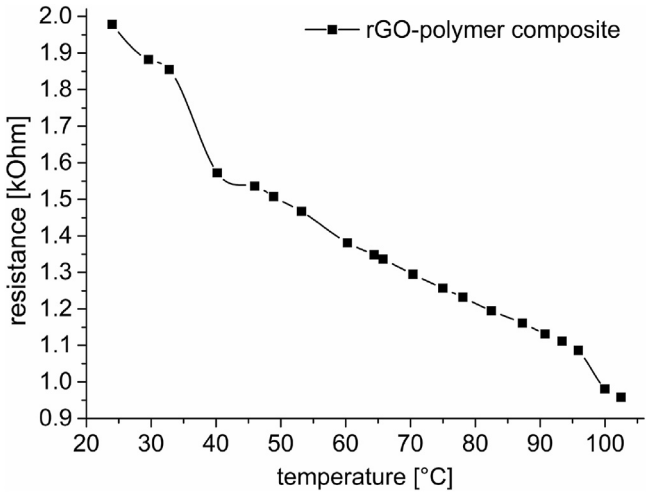

Fig. 4. Resistance of rGO-PEDOT:PSS polymer composition depending on temperature in the range of 20–110°C in air.

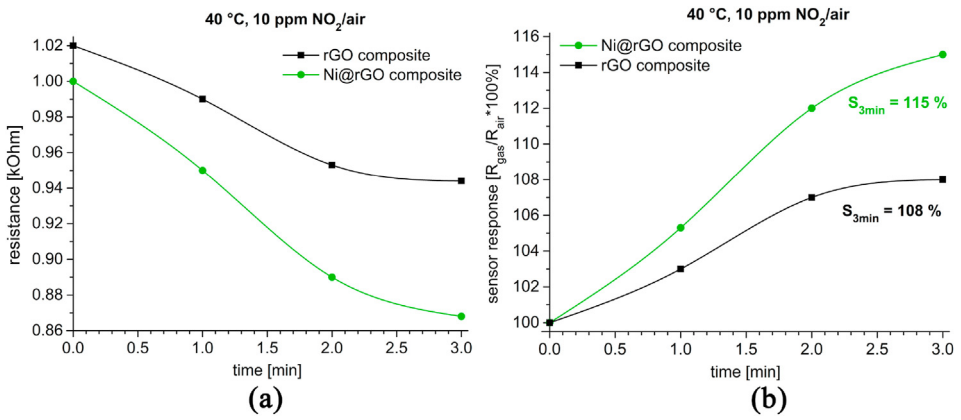

Fig. 5. Dependence of electrical resistance (a) and sensor response (b) of the Ni@rGO (green) and rGO (black) PEDOT:PSS composite on the time of exposure to a gas-air mixture containing 10 ppm NO_2. Response time: 3 min.

40 °C, the sensor response was $S = 108\%$ for the rGO-PEDOT:PSS polymer composite and $S = 115\%$ for the Ni@rGO-PEDOT:PSS composite (Fig. 5b), which is already of practical interest. For example, semiconductor metal oxide sensors exhibit a comparable sensor response, but at higher temperatures, above 100 °C [60]. The nature of gas response in our case corresponds to *p*-type conductivity (a decrease in resistance when exposed to an oxidizing gas).

In our measuring chamber, based on an estimate of the extrapolation of the NO_2 concentration value to the minimum value of the acceptable detectable signal, the detection limit should be ~1 ppm. This is less than and therefore provides an enhancement over the limit reported in works of single-layer graphene [61], WO_3 + rGO [62], SnO_2 + rGO [63], rGO + ZnO [64], SnO_2 + rGO [65], WO_3 + rGO [11] or GR/PMMMA [66]. At the same time, compared to studies of graphene [67], rGO/($FeCl_3$ + Fe_2O_3) [68], GO + Cs [69] or ozone-treated graphene [70] our NO_2 detection limit turned out to be higher. For studies of multilayer graphene [71] or NiO + rGO [7] the detection limit for NO_2 was similar to ours.

The response time of 3 min for film type sensors is very low. Lower values were noted only in studies of rGO + NiO [7] and rGO + ZnO [64]. In all the other references cited above, the response time of the sensors is longer compared to ours with up to 60 min for single-layer graphene [61]. The closest response time to our value of 180 s is given for a graphene-polymer composition [66] with a response time of 170 s.

At temperatures above 110°C, the polymer contained in the composition irreversibly loses its conductive properties and already performs only the role of an adhesive additive (Fig. 6).

At temperatures above 100 °C, the electrical resistance of the gas-sensitive layer formed after thermal destruction of the polymer was measured. The gas-sensitive layer was previously subjected to stabilization annealing at 210 °C for 2 h. The sensor response of electrical resistance was determined for a mixture of 35,000 ppm acetone vapor in air at 195 °C (Fig. 7), 3000 ppm CO in nitrogen at 195 °C (Fig. 8), 10 ppm NO_2 in air at 197 °C (Fig. 9). The response time and recovery time determined under the dynamic conditions of the experiment for an atmosphere of 3000 ppm CO in nitrogen are T_{res} ~17 min and T_{rec}~2 min, respectively.

The nature of the gas response of the material after thermal destruction of the polymer and stabilization annealing of the gas-sensitive layer corresponds to *n*-type conductivity (an increase in resistance when NO_2 is applied and a decrease in resistance when reducing agent vapors occurs).

It should be noted that the ternary material mixture system based on the conductive polymer PEDOT:PSS is not a simple combination. In order to realize the synergistic effect of various materials, process compatibility, morphology, structure etc. should be taken into account. For example, when detecting gases of a reducing nature from the group of hydrocarbons, CO, acetone etc. with film-type sensors containing

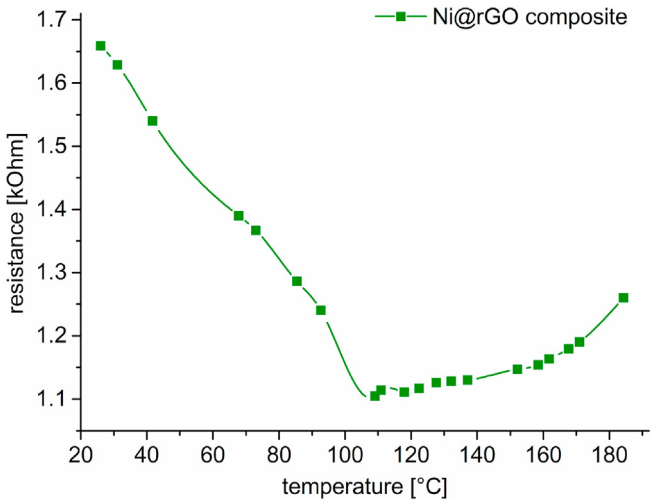

Fig. 6. Electrical resistance of Ni@rGO-PEDOT:PSS polymer composition, depending on temperature in the range of 20–190°C in air.

graphene and polymer, it turns out that the response and recovery times are usually lower than for gases of an oxidizing nature [17]. At the same time, for sensors of graphene-metal oxide structures, such a difference almost does not exist. The same is observed for our sensors.

There are not many publications devoted to sensors of film structures of metal@graphene with polymer. For our system Ni@rGO-PEDOT:PSS polymer which was used for the analysis of the gases NO_2, CO and the vapor acetone, we are not aware of previous publications to the best of our knowledge. Therefore, there remains only an opportunity to compare the operation of sensors in terms of their conditions, their composition and analyzed gases as close as possible. It should be borne in mind that the operating conditions of our sensors for CO and acetone differ significantly from those found in the literature [17,59] at the present time. Although, for example, when detecting for NO_2 our sensor in terms of the response parameter (response ~130%) is even similar to the indicators of the sensor of ZnO-graphene composition (response ~135%) [64]. The response time in our case for CO is about 12 min. In comparison, functionalized rGO gives a response in 4 min, while using only 30 ppm CO at room temperature [72]. In the case of acetone, after 10 min of exposure, a saturation of the sensor response curve in our case is not observed, therefore, it is not possible to assume the true value of the response and response time. The response can be significantly higher than 107%. We have only succeeded in showing the very fact that the sensitivity of the Ni@rGO-PEDOT:PSS polymer film system to acetone is quite sufficient for practice. From the review in Ref. [59] we also see that

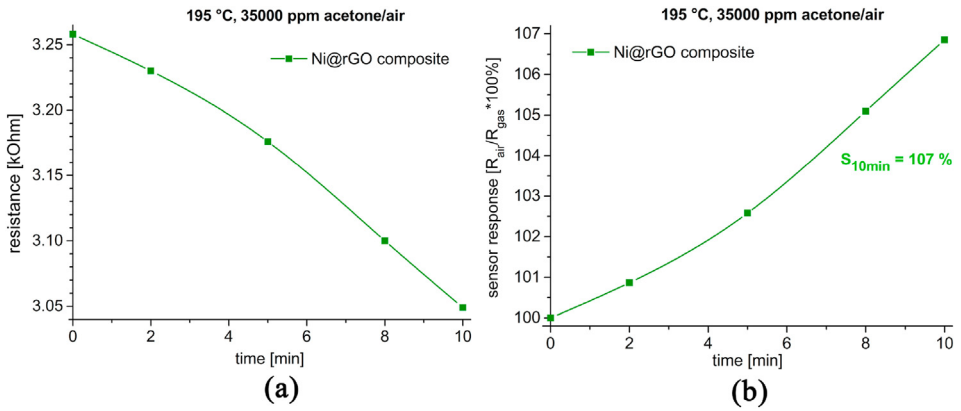

Fig. 7. Dependence of electrical resistance (a) and sensor response (b) of the Ni@rGO-PEDOT:PSS composite on the time of exposure to a gas-air mixture containing 35,000 ppm acetone vapor.

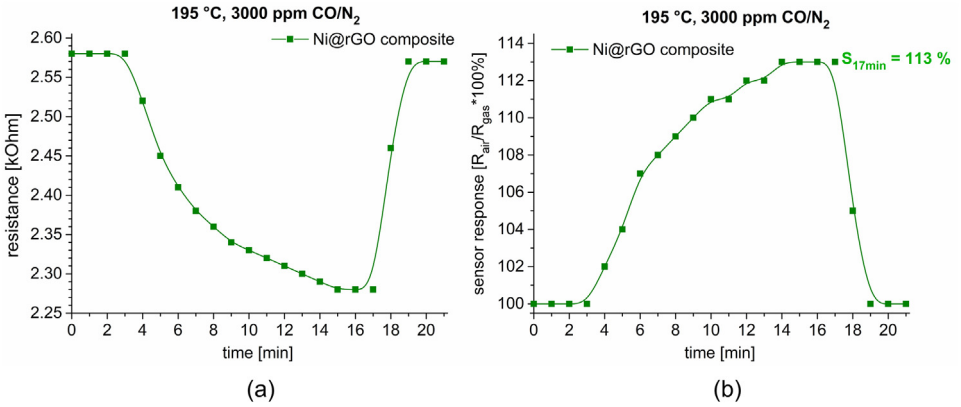

Fig. 8. Dependence of electrical resistance (a) and sensor response (b) of the Ni@rGO-PEDOT:PSS composite on the time of exposure to a gas mixture containing 3000 ppm CO in nitrogen. Response time: ~17 min, recovery time: ~2 min.

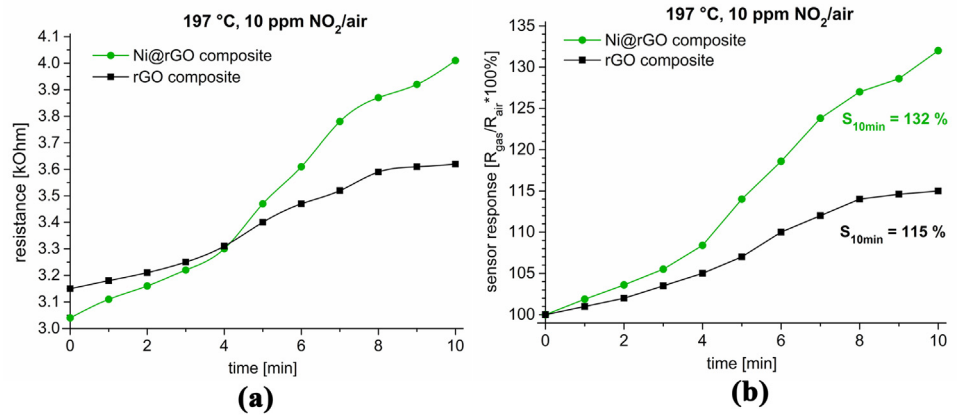

Fig. 9. Dependence of electrical resistance (a) and sensor response (b) of the Ni@rGO-(green) and rGO-(black) PEDOT:PSS composite on the time of exposure to a gas-air mixture containing 10 ppm NO_2 in air. Response time: ~10 min.

low response times are characteristic for sensors made of metal oxide compositions (for example, ref. [73] - 4 s, ref. [74] - 10 s), and in all cases of graphene-polymer compositions this value is significantly higher (ref. [75] - 18 min, ref. [76] - 5 min). Thus, in summary, we can say that in terms of NO_2 our system looks among the best, while in terms of reducing gases it is difficult to make a comparison due to different experimental conditions.

When considering the possible mechanism for the influence of nickel on the sensor properties, in addition to selective catalytic activity, it is also possible to draw on the existing explanation for the interaction of clusters of metal particles with a semiconductor. This interaction is called the spillover effect [77,78]. It is known that for metals with a large work function of electrons, such as Ag (4.7 eV), Pd (5.0 eV), Pt (5.3 eV), a large barrier height leads to a wide depletion zone. For nickel the work function is 4.91–5.1 eV [79]. When interacting with a gas atom, the barrier height at the Ni@rGO interface decreases due to the spillover effect (electron transfer), which leads to a greater decrease in resistance than in the case of rGO alone. For these processes to be effective, nickel particles

must be very small in diameter, there should be a large number of particles and the nickel particles should be evenly distributed in the rGO volume. In addition, the effect can be enhanced by a large specific surface area of the material, which is the case for rGO. Moreover, it is possible that the interaction between nickel and graphene is the main reason for the faster response and higher sensitivity of the Ni@rGO contact resistance compared to rGO resistance. It was reported that the interaction between nickel atoms and π-orbitals in graphene strongly distorts the graphene lattice and will introduce graphene edge defects into the graphene lattice [37].

4. Conclusion

Through investigations of the structure and composition and most importantly the properties, neat Ni@rGO nanocomposites were found to be promising materials with high-effective sensing abilities that enable the construction of elements for gas sensors with enhanced properties. Thus, it was found that the studied Ni@rGO-PEDOT:PSS composite material is sensitive to gases of various chemical nature, and, to a much greater extent, to oxidizing gases (NO_2). A comparison with the metal-free rGO-PEDOT:PSS polymer composite shows that the Ni@rGO-PEDOT:PSS composite gives better results for NO_2 gas. The results of the measurements already allow us to suggest regimes for the formation of gas-sensitive layers of Ni@rGO for commercially available low-power film sensors using substrates of Al_2O_3. The thermal stability of nickel nanoparticles after heat treatment was confirmed by powder diffraction.

Declaration of competing interest

The authors declare no conflict of interest.

Acknowledgements

Authors are thankful to the Deutsche Forschungsgemeinschaft (DFG) for financial support within the priority project SPP 1708 through grant Ja466/31-1, Ja466/31-2. We thank the Ernst Ruska-Centre (Forschungszentrum Jülich GmbH, Jülich, Germany) and Dr. Juri Barthel for access to the TEM facility and technical support under project number ER-C D-066 and in the core-facilities program through grant MA 1280/40-1.

Appendix A. Supplementary data

Supplementary data to this article can be found online at https://doi.org/10.1016/j.nanoms.2021.03.004.

References

[1] F.-L. Meng, Z. Guo, X.-J. Huang, Trends Anal. Chem. 68 (2015) 37–47, https://doi.org/10.1016/j.trac.2015.02.008.
[2] D. Nunes, A. Pimentel, A. Gonçalves, S. Pereira, R. Branquinho, P. Barquinha, E. Fortunato, R. Martins, Semicond. Sci. Technol. 34 (2019) 43001–44001, https://doi.org/10.1088/1361-6641/ab011e.
[3] K. Wetchakun, T. Samerjai, N. Tamaekong, C. Liewhiran, C. Siriwong, V. Kruefu, A. Wisitsoraat, A. Tuantranont, S. Phanichphant, Sens. Actuator. B Chem. 160 (2011) 580–591, https://doi.org/10.1016/j.snb.2011.08.032.
[4] G. Jeevitha, R. Abhinayaa, D. Mangalaraj, N. Ponpandian, P. Meena, V. Mounasamy, S. Madanagurusamy, Nanoscale Adv. 1 (2019) 1799–1811, https://doi.org/10.1039/C9NA00048H.
[5] W. Tian, X. Liu, W. Yu, Appl. Sci. 8 (2018) 1118–1138, https://doi.org/10.3390/app8071118.
[6] S.S. Varghese, S. Lonkar, K.K. Singh, S. Swaminathan, A. Abdala, Sens. Actuator. B Chem. 218 (2015) 160–183, https://doi.org/10.1016/j.snb.2015.04.062.
[7] T. Le Hoa, H.N. Tien, H. van Luan, J.S. Chung, S.H. Hur, Sens. Actuator. B Chem. 185 (2013) 701–705, https://doi.org/10.1016/j.snb.2013.05.050.
[8] S. Basu, P. Bhattacharyya, Sens. Actuator. B Chem. 173 (2012) 1–21, https://doi.org/10.1016/j.snb.2012.07.092.
[9] J. Zhang, H. Lu, C. Yan, Z. Yang, G. Zhu, J. Gao, F. Yin, C. Wang, Sens. Actuator. B Chem. 264 (2018) 128–138, https://doi.org/10.1016/j.snb.2018.02.026.
[10] V.S. Bhati, S. Ranwa, S. Rajamani, K. Kumari, R. Raliya, P. Biswas, M. Kumar, ACS Appl. Mater. Interfaces 10 (2018) 11116–11124, https://doi.org/10.1021/acsami.7b17877.
[11] P.-G. Su, S.-L. Peng, Talanta 132 (2015) 398–405, https://doi.org/10.1016/j.talanta.2014.09.034.
[12] X. Zhou, T. Wu, K. Ding, B. Hu, M. Hou, B. Han, Chem. Commun. 46 (2010) 386–388, https://doi.org/10.1039/b914763b.
[13] B. Zhang, W. Ning, J. Zhang, X. Qiao, J. Zhang, J. He, C.-Y. Liu, J. Mater. Chem. 20 (2010) 5401–5403, https://doi.org/10.1039/c0jm01029d.
[14] V.V. Chaban, E.E. Fileti, RSC Adv. 5 (2015) 81229–81234, https://doi.org/10.1039/C5RA16857K.
[15] X. Wang, P.F. Fulvio, G.A. Baker, G.M. Veith, R.R. Unocic, S.M. Mahurin, M. Chi, S. Dai, Chem. Commun. 46 (2010) 4487–4489, https://doi.org/10.1039/c0cc00799d.
[16] D. Nuvoli, L. Valentini, V. Alzari, S. Scognamillo, S.B. Bon, M. Piccinini, J. Illescas, A. Mariani, J. Mater. Chem. 21 (2011) 3428–3431, https://doi.org/10.1039/C0JM02461A.
[17] D. Sun, Y. Luo, M. Debliquy, C. Zhang, Beilstein J. Nanotechnol. 9 (2018) 2832–2844, https://doi.org/10.3762/bjnano.9.264.
[18] S. Mao, G. Lu, K. Yu, Z. Bo, J. Chen, Adv. Mater. 22 (2010) 3521–3526, https://doi.org/10.1002/adma.201000520.
[19] P.T. Yin, S. Shah, M. Chhowalla, K.-B. Lee, Chem. Rev. 115 (2015) 2483–2531, https://doi.org/10.1021/cr500537t.
[20] Y. Xia, R. Li, R. Chen, J. Wang, L. Xiang, Sensors 18 (2018) 1456–1477, https://doi.org/10.3390/s18051456.
[21] W. Qu, H. Bao, L. Zhang, G. Chen, Chem. Eur J. 18 (2012) 15746–15752, https://doi.org/10.1002/chem.201202913.
[22] T. Welton, Chem. Rev. 99 (1999) 2071–2084, https://doi.org/10.1021/cr980032t.
[23] C. Chiappe, D. Pieraccini, J. Phys. Org. Chem. 18 (2005) 275–297, https://doi.org/10.1002/poc.863.
[24] F. Davar, Z. Fereshteh, M. Salavati-Niasari, J. Alloys Compd. 476 (2009) 797–801, https://doi.org/10.1016/j.jallcom.2008.09.121.
[25] A.P. LaGrow, B. Ingham, M.F. Toney, R.D. Tilley, J. Phys. Chem. C 117 (2013) 16709–16718, https://doi.org/10.1021/jp405314g.
[26] S. Wegner, C. Rutz, K. Schütte, J. Barthel, A. Bushmelev, A. Schmidt, K. Dilchert, R.A. Fischer, C. Janiak, Chem. Eur J. 23 (2017) 6330–6340, https://doi.org/10.1002/chem.201605251.
[27] K. Gotoh, K. Kawabata, E. Fujii, K. Morishige, T. Kinumoto, Y. Miyazaki, H. Ishida, Carbon 47 (2009) 2120–2124, https://doi.org/10.1016/j.carbon.2009.03.052.
[28] D. Marquardt, C. Vollmer, R. Thomann, P. Steurer, R. Mülhaupt, E. Redel, C. Janiak, Carbon 49 (2011) 1326–1332, https://doi.org/10.1016/j.carbon.2010.09.066.
[29] R. Marcos Esteban, K. Schütte, D. Marquardt, J. Barthel, F. Beckert, R. Mülhaupt, C. Janiak, Nano-Struct. Nano-Objects 2 (2015) 28–34, https://doi.org/10.1016/j.nanoso.2015.07.002.
[30] R. Marcos Esteban, K. Schütte, P. Brandt, D. Marquardt, H. Meyer, F. Beckert, R. Mülhaupt, H. Kölling, C. Janiak, Nano-Struct. Nano-Objects 2 (2015) 11–18, https://doi.org/10.1016/j.nanoso.2015.07.001.
[31] D. Marquardt, F. Beckert, F. Pennetreau, F. Tölle, R. Mülhaupt, O. Riant, S. Hermans, J. Barthel, C. Janiak, Carbon 66 (2014) 285–294, https://doi.org/10.1016/j.carbon.2013.09.002.
[32] A. Schmitz, K. Schütte, V. Ilievski, J. Barthel, L. Burk, R. Mülhaupt, J. Yue, B. Smarsly, C. Janiak, Beilstein J. Nanotechnol. 8 (2017) 2474–2483, https://doi.org/10.3762/bjnano.8.247.
[33] A. Kaniyoor, R. Imran Jafri, T. Arockiadoss, S. Ramaprabhu, Nanoscale 1 (2009) 382–386, https://doi.org/10.1039/b9nr00015a.
[34] M.G. Chung, D.-H. Kim, D.K. Seo, T. Kim, H.U. Im, H.M. Lee, J.-B. Yoo, S.-H. Hong, T.J. Kang, Y.H. Kim, Sens. Actuator. B Chem. 169 (2012) 387–392, https://doi.org/10.1016/j.snb.2012.05.031.
[35] W. Li, X. Geng, Y. Guo, J. Rong, Y. Gong, L. Wu, X. Zhang, P. Li, J. Xu, G. Cheng, M. Sun, L. Liu, ACS Nano 5 (2011) 6955–6961, https://doi.org/10.1021/nn201433r.
[36] W. Qu, L. Zhang, G. Chen, Biosens. Bioelectron. 42 (2013) 430–433, https://doi.org/10.1016/j.bios.2012.11.011.
[37] Q. Li, W. Liu, G. Cao, X. Li, X. Wang, Appl. Phys. Lett. 108 (2016) 221604–221607, https://doi.org/10.1063/1.4952619.
[38] H. Wu, Q. Li, X. Bu, W. Liu, G. Cao, X. Li, X. Wang, Sens. Actuator. B Chem. 282 (2019) 408–416, https://doi.org/10.1016/j.snb.2018.11.066.
[39] P. Bonhôte, A.-P. Dias, N. Papageorgiou, K. Kalyanasundaram, M. Grätzel, Inorg. Chem. 35 (1996) 1168–1178, https://doi.org/10.1021/ic951325x.
[40] A.K. Burrell, R.E.D. Sesto, S.N. Baker, T.M. McCleskey, G.A. Baker, Green Chem. 9 (2007) 449–454, https://doi.org/10.1039/b615950h.
[41] W.S. Hummers, R.E. Offeman, J. Am. Chem. Soc. 80 (1958) 1339, https://doi.org/10.1021/ja01539a017.
[42] M. Luysberg, M. Heggen, K. Tillmann, Ernst Ruska-centre for microscopy and spectroscopy with electrons, FEI Tecnai G2 F20, JLSRF J. Large-scale Res. Facil. 2 (2016) A77, https://doi.org/10.17815/jlsrf-2-138.
[43] A. Thust, J. Barthel, K. Tillmann, Ernst Ruska-centre for microscopy and spectroscopy with electrons. FEI Titan 80-300 TEM, JLSRF J. Large-scale Res. Facil. 2 (2016) A41, https://doi.org/10.17815/jlsrf-2-66.
[44] J. Dupont, J.D. Scholten, Chem. Soc. Rev. 39 (2010) 1780–1804, https://doi.org/10.1039/b822551f.
[45] P. Wasserscheid, W. Keim, Angew. Chem. 112 (2000) 3926–3945, https://doi.org/10.1002/1521-3757(20001103)112:21<3926:AID-ANGE3926>3.0.CO;2-U. Angew. Chem. Int. Ed. 2000, 39, 3772–3789. doi:10.1002/1521-3773(20001103)39:21%3C3772:AID-ANIE3772%3E3.0.CO;2-5.

[46] J. Dupont, J. Braz. Chem. Soc. 15 (2004) 341–350, https://doi.org/10.1590/S0103-50532004000300002.
[47] C. Janiak, Metal nanoparticle synthesis in ionic liquids, in: J. Dupont, L. Kollár (Eds.), Ionic Liquids (ILs) in Organometallic Catalysis, Springer Berlin Heidelberg, Berlin, Heidelberg, 2015, pp. 17–53.
[48] K. Schütte, J. Barthel, M. Endres, M. Siebels, B.M. Smarsly, J. Yue, C. Janiak, ChemistryOpen 6 (2017) 137–148, https://doi.org/10.1002/open.201600105.
[49] M. Siebels, L. Mai, L. Schmolke, K. Schütte, J. Barthel, J. Yue, J. Thomas, B.M. Smarsly, A. Devi, R.A. Fischer, C. Janiak, Beilstein J. Nanotechnol. 9 (2018) 1881–1894, https://doi.org/10.3762/bjnano.9.180.
[50] D.R. Dreyer, S. Park, C.W. Bielawski, R.S. Ruoff, Chem. Soc. Rev. 39 (2010) 228–240, https://doi.org/10.1039/b917103g.
[51] F.J. Tölle, M. Fabritius, R. Mülhaupt, Adv. Funct. Mater. 22 (2012) 1136–1144, https://doi.org/10.1002/adfm.201102888.
[52] G. Goncalves, P.A.A.P. Marques, C.M. Granadeiro, H.I.S. Nogueira, M.K. Singh, J. Grácio, Chem. Mater. 21 (2009) 4796–4802, https://doi.org/10.1021/cm901052s.
[53] C.V. Pham, M. Eck, M. Krueger, Chem. Eng. J. 231 (2013) 146–154, https://doi.org/10.1016/j.cej.2013.07.007.
[54] M. Ma, J. Zhang, W. Shen, S.J. Guo, Solid State Electrochem. 23 (2019) 2969–2977, https://doi.org/10.1007/s10008-019-04390-7.
[55] S.C. Lee, H.Y. Choi, S.J. Lee, W.S. Lee, J.S. Huh, D.D. Lee, J.C. Kim, Sens. Actuator. B Chem. 138 (2009) 446–452, https://doi.org/10.1016/j.snb.2009.02.064.
[56] T. Kida, A. Nishiyama, M. Yuasa, K. Shimanoe, N. Yamazoe, Sens. Actuator. B Chem. 135 (2009) 568–574, https://doi.org/10.1016/j.snb.2008.09.056.
[57] S.J. Ippolito, S. Kandasamy, K. Kalantar-zadeh, W. Wlodarski, Sens. Actuator. B Chem. 108 (2005) 154–158, https://doi.org/10.1016/j.snb.2004.11.092.
[58] N. Barsan, D. Koziej, U. Weimar, Sens. Actuator. B Chem. 121 (2007) 18–35, https://doi.org/10.1016/j.snb.2006.09.047.
[59] T. Wang, D. Huang, Z. Yang, S. Xu, G. He, X. Li, N. Hu, G. Yin, D. He, L. Zhang, Nano-Micro Lett. 8 (2016) 95–119, https://doi.org/10.1007/s40820-015-0073-1.
[60] X. Chu, T. Hu, F. Gao, Y. Dong, W. Sun, L. Bai, Mater. Sci. Eng. B 193 (2015) 97–104, https://doi.org/10.1016/j.mseb.2014.11.011.
[61] R. Pearce, T. Iakimov, M. Anderssons, L. Hultman, A.L. Spetz, R. Yakimova, Sens. Actuator. B Chem. 155 (2011) 451–455, https://doi.org/10.1016/j.snb.2010.12.046.
[62] S. Srivastava, K. Jain, V.N. Singh, S. Singh, N. Vijayan, N. Dilawar, G. Gupta, T.D. Senguttuvan, Nanotechnology 23 (2012) 205501–205507, https://doi.org/10.1088/0957-4484/23/20/205501.
[63] X. Liu, J. Cui, J. Sun, X. Zhang, RSC Adv. 4 (2014) 22601–22605, https://doi.org/10.1039/C4RA02453B.
[64] S. Liu, B. Yu, H. Zhang, T. Fei, T. Zhang, Sens. Actuator. B Chem. 202 (2014) 272–278, https://doi.org/10.1016/j.snb.2014.05.086.
[65] H. Zhang, J. Feng, T. Fei, S. Liu, T. Zhang, Sens. Actuator. B Chem. 190 (2014) 472–478, https://doi.org/10.1016/j.snb.2013.08.067.
[66] C. Lee, J. Ahn, K.B. Lee, D. Kim, J. Kim, Thin Solid Films 520 (2012) 5459–5462, https://doi.org/10.1016/j.tsf.2012.03.095.
[67] F. Yavari, E. Castillo, H. Gullapalli, P.M. Ajayan, N. Koratkar, Appl. Phys. Lett. 100 (2012) 203120, https://doi.org/10.1063/1.4720074.
[68] Y. Dong, X. Zhang, X. Cheng, Y. Xu, S. Gao, H. Zhao, L. Huo, RSC Adv. 4 (2014) 57493–57500, https://doi.org/10.1039/C4ra10136g.
[69] C. Piloto, M. Notarianni, M. Shafiei, E. Taran, D. Galpaya, C. Yan, N. Motta, Beilstein J. Nanotechnol. 5 (2014) 1073–1081, https://doi.org/10.3762/bjnano.5.120.
[70] M.G. Chung, D.H. Kim, H.M. Lee, T. Kim, J.H. Choi, D.K. Seo, J.-B. Yoo, S.-H. Hong, T.J. Kang, Y.H. Kim, Sens. Actuator. B Chem. 166–167 (2012) 172–176, https://doi.org/10.1016/j.snb.2012.02.036.
[71] H. Choi, H.Y. Jeong, D.-S. Lee, C.-G. Choi, S.-Y. Choi, Carbon Lett. 14 (2013) 186–189, https://doi.org/10.5714/Cl.2013.14.3.186.
[72] D. Panda, A. Nandi, S.K. Datta, H. Saha, S. Majumdar, RSC Adv. 6 (2016) 47337–47348, https://doi.org/10.1039/C6RA06058G.
[73] F. Liu, X. Chu, Y. Dong, W. Zhang, W. Sun, L. Shen, Sens. Actuator. B Chem. 188 (2013) 469–474, https://doi.org/10.1016/j.snb.2013.06.065.
[74] Z. Jiang, J. Wang, L. Meng, Y. Huang, L. Liu, Chem. Commun. 47 (2011) 6350–6352, https://doi.org/10.1039/c1cc11711d.
[75] N. Hu, Y. Wang, J. Chai, R. Gao, Z. Yang, E.S.-W. Kong, Y. Zhang, Sens. Actuator. B Chem. 163 (2012) 107–114, https://doi.org/10.1016/j.snb.2012.01.016.
[76] B. Chen, H. Liu, X. Li, C. Lu, Y. Ding, B. Lu, Appl. Surf. Sci. 258 (2012) 1971–1975, https://doi.org/10.1016/j.apsusc.2011.05.101.
[77] A. Sholehah, D.F. Faroz, N. Huda, L. Utari, N.L.W. Septiani, B. Yuliarto, Chemosensors 8 (2020) 2, https://doi.org/10.3390/chemosensors8010002.
[78] M. Hübner, D. Koziej, J.-D. Grunwaldt, U. Weimar, N. Barsan, Phys. Chem. Chem. Phys. 14 (2012) 13249–13254, https://doi.org/10.1039/c2cp41349c.
[79] S. Halas, T. Durakiewicz, J. Phys. Condens. Matter 10 (1998) 10815–10826, https://doi.org/10.1088/0953-8984/10/48/005.